Inorg. Chem. **2005**, *44*, 1211–1220

Luminescent Platinum(II) Dimers with a Cyclometallating Aryldiamine Ligand

Hershel Jude, Jeanette A. Krause Bauer, and William B. Connick*

Department of Chemistry, University of Cincinnati, P.O. Box 210172, Cincinnati, Ohio 45221-0172

Received June 26, 2004

Triflate salts of three $(Pt(pip_2NCN))_2(\mu\text{-}L)^{2+}$ (pip_2NCNH = 1,3-bis(piperidylmethyl)benzene) dimers bridged by a series of nitrogen-donor ligands (L = pyrazine (pyz), 1,2-bis(4-pyridyl)ethane (bpa), *trans*-1,2-bis(4-pyridyl)ethylene (bpe)) are reported. These complexes have been fully characterized by ^{1}H NMR spectroscopy and elemental analysis. The X-ray crystal structures of $[(Pt(pip_2NCN))_2(\mu\text{-pyz})](CF_3SO_3)_2$ and $[(Pt(pip_2NCN))_2(\mu\text{-bpe})](CF_3SO_3)_2\cdot 2CH_2Cl_2$ are reported. $[(Pt(pip_2NCN))_2(\mu\text{-pyz})](CF_3SO_3)_2$: triclinic, $P\bar{1}$, $a = 12.5240(5)$ Å, $b = 14.1570(6)$ Å, $c = 14.2928(6)$ Å, $\alpha = 106.458(1)°$, $\beta = 92.527(1)°$, $\gamma = 106.880(1)°$, $V = 2303.46(17)$ Å^3, $Z = 2$. $[(Pt(pip_2NCN))_2(\mu\text{-bpe})](CF_3SO_3)_2\cdot 2CH_2Cl_2$: monoclinic, $P2_1/c$, $a = 10.1288(6)$ Å, $b = 16.3346(9)$ Å, $c = 17.4764(10)$ Å, $\beta = 90.882(2)°$, $V = 2891.1(3)$ Å^3, $Z = 2$. These structures and solution measurements provide evidence for the strong trans-directing properties of the pip_2NCN^- ligand. The electronic structures of these complexes and those of the 4,4′-bipyridine (bpy) dimer, $(Pt(pip_2NCN))_2(\mu\text{-bpy})^{2+}$, also have been investigated by UV–visible absorption and emission spectroscopies, as well as cyclic voltammetry. The accumulated data indicate that variations in the bridging ligands provide remarkable control over the electronic structures and photophysics of these complexes. Notably, the bpa dimer exhibits a broad, low-energy emission from a metal-centered ^{3}LF excited state, whereas the bpe and bpy dimers exhibit structured emission from a lowest pyridyl-centered $^3(\pi\text{–}\pi^*)$ excited state. In contrast, the pyz dimer exhibits remarkably intense yellow emission tentatively assigned to a triplet metal-to-ligand charge-transfer excited state.

Introduction

During the past 15 years, there has been increasing interest in using pyrazine (pyz),[1−5] *trans*-1,2-bis(4-pyridyl)ethylene (bpe),[6−14] 1,2-bis(4-pyridyl)ethane (bpa),[15,16] and 4,4′-bipyridine (bpy)[8,10−13,16−23] as building blocks for supramolecular platinum complexes.

Complexes with these ligands tend to self-assemble[4,6−8,20−22] and have potentially useful medicinal,[2,3,13−16] photochemical,[10,23,24] and electrochemical[10,11,23,24] properties. While supramolecular structures, such as $(Pt(PMe_3)_2(\mu\text{-bpe}))_4^{8+}$,

* To whom correspondence should be addressed. E-mail: bill.connick@uc.edu.

(1) Albinati, A.; Isaia, F.; Kaufmann, W.; Sorato, C.; Venanzi, L. M. *Inorg. Chem.* **1989**, *28*, 1112−1122.
(2) Komeda, S.; Kalayda, G. V.; Lutz, M.; Spek, A. L.; Yamanaka, Y.; Sato, T.; Chikuma, M.; Reedijk, J. *J. Med. Chem.* **2003**, *46*, 1210−1219.
(3) Kumazawa, K.; Biradha, K.; Kusukawa, T.; Okano, T.; Fujita, M. *Angew. Chem., Int. Ed.* **2003**, *42*, 3909−3913.
(4) Schweiger, M.; Seidel, S. R.; Arif, A. M.; Stang, P. J. *Angew. Chem., Int. Ed.* **2001**, *40*, 3467−3469.
(5) Lu, W.; Chan, M. C. W.; Cheung, K.-K.; Che, C.-M. *Organometallics* **2001**, *20*, 2477−2486.
(6) Kryschenko, Y. K.; Seidel, S. R.; Arif, A. M.; Stang, P. J. *J. Am. Chem. Soc.* **2003**, *125*, 5193−5198.
(7) Schweiger, M.; Seidel, S. R.; Arif, A. M.; Stang, P. J. *Inorg. Chem.* **2002**, *41*, 2556−2559.
(8) Schalley, C. A.; Muller, T.; Linnartz, P.; Witt, M.; Schafer, M.; Lutzen, A. *Chem.—Eur. J.* **2002**, *8*, 3538−3551.
(9) Chen, W.; Liu, X.; You, X. *Chem. Lett.* **2002**, 734−735.
(10) Sun, S.-S.; Anspach, J. A.; Lees, A. J. *Inorg. Chem.* **2002**, *41*, 1862−1869.
(11) Kaim, W.; Schwederski, B.; Dogan, A.; Fiedler, J.; Kuehl, C. J.; Stang, P. J. *Inorg. Chem.* **2002**, *41*, 4025−4028.
(12) Kuehl, C. J.; Arif, A. M.; Stang, P. J. *Org. Lett.* **2000**, *2*, 3727−3729.
(13) Lowe, G.; Droz, A. S.; Vilaivan, T.; Weaver, G. W.; Park, J. J.; Pratt, J. M.; Tweedale, L.; Kelland, L. R. *J. Med. Chem.* **1999**, *42*, 3167−3174.
(14) Lowe, G.; McCloskey, J. A.; Ni, J.; Valaivan, T. *Bioorg. Med. Chem.* **1996**, *4*, 1007−1013.
(15) Brown, D. B.; Khokhar, A. R.; Hacker, M. P.; Lokys, L.; Burchenal, J. H.; Newman, R. A.; McCormack, J. J. *J. Med. Chem.* **1982**, *25*, 952−956.
(16) Cafeo, G.; Lo Passo, C.; Scolaro, L. M.; Pernice, I.; Romeo, R. *Inorg. Chim. Acta* **1998**, *275*, 141−149.
(17) Orita, A.; Jiang, L.; Nakano, T.; Ma, N.; Otera, J. *Chem. Commun.* **2002**, 1362−1363.
(18) Fujita, M.; Ibukuro, F.; Yamaguchi, K.; Ogura, K. *J. Am. Chem. Soc.* **1995**, *117*, 4175−4176.

10.1021/ic049166h CCC: $30.25
Published on Web 01/25/2005

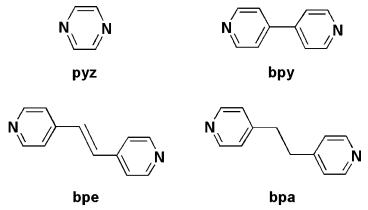

$(Pt(PMe_3)_2(\mu\text{-bpe}))_3^{6+}$, and $(Pt(PMe_3)_2(\mu\text{-pyz}))_3^{6+}$ prepared by Stang's group,[4,7] have received increasing attention, platinum(II) dimers bridged by pyz,[1,2,5] bpy,[23−26] bpe,[13,14] and bpa[16] are comparatively rare.

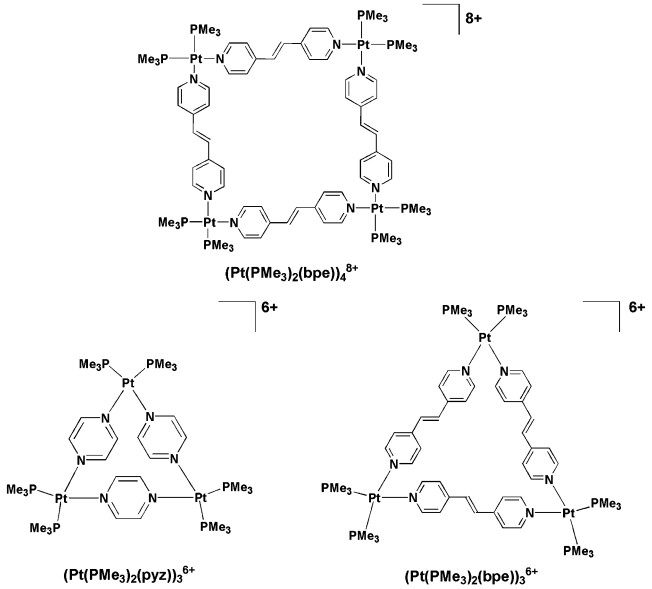

In our earlier investigations, focused on the electronic structures of square planar platinum(II) monomers with the tridentate pincer ligand pip_2NCN^-,[27,28] we found that variation of the monodentate ligand provides remarkable control over the electronic structures of this class of compounds. Notably, luminescence (λ_{max} = 705 nm) from $Pt(pip_2NCN)Cl$ originates from a lowest, predominantly spin-forbidden ligand field (^{3}LF) state, whereas structured emission (λ_{max} = 444, 474, 498 nm) from $Pt(pip_2NCN)(phpy)^+$ (phpy = 4-phenylpyridine) originates from a lowest phpy-centered $^3(\pi-\pi^*)$ excited state. With the notion that the $Pt(pip_2NCN)$ fragment will prefer to form dimers over more elaborate architectures, such as triangles and squares, we have undertaken the synthesis of a series of $(Pt(pip_2NCN))_2(\mu\text{-L})^{2+}$ complexes (L = pyz, bpa, bpy, or bpe). Here, we discuss the electronic structures of these complexes and compare these properties to related systems. Our findings demonstrate that modifications of the bridging ligand provide exquisite control over the electronic structures and photophysics of these compounds, including the orbital character of the lowest emissive state.

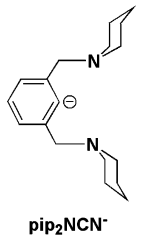

Experimental Section

Tetrahydrofuran (THF) was distilled from Na(s)/benzophenone, ethanol was distilled from zinc metal/potassium hydroxide, and methylene chloride was distilled from CaH_2. Anhydrous 2-methyltetrahydrofuran (2-MeTHF) was purchased from Aldrich Chemical Co. (Milwaukee, WI) and used as received. All other reagents were purchased from Acros (Somerville, NJ) and used as received. $Pt(pip_2NCN)Cl$ and $[Pt(pip_2NCN)(\mu\text{-bpy})](CF_3SO_3)_2$ were prepared as previously described.[27,28] Tetrabutylammonium hexafluorophosphate ($TBAPF_6$) was recrystallized twice from boiling methanol and dried under vacuum prior to use. Argon was predried using activated sieves, and trace impurities of oxygen were removed with activated R3-11 catalyst from Schweizerhall (New Jersey).

^{1}H NMR spectra were recorded at room temperature using a Bruker AC 250 MHz spectrometer. Deuterated chloroform (0.03% tetramethylsilane (TMS)), methanol, and acetonitrile were purchased from Cambridge Isotope Laboratories (Andover, MA). UV−visible absorption spectra were recorded using a HP8453 UV−visible spectrometer. Cyclic voltammetery was carried out using a standard three-electrode cell and a CV50w potentiostat from Bioanalytical Systems. Scans were collected in methylene chloride solution containing 0.1 M $TBAPF_6$. All scans were recorded using a platinum wire auxiliary electrode, a Ag/AgCl (3.0 M NaCl) reference electrode, and a 0.79 mm^2 gold working electrode. Between scans, the working electrode was polished with 0.05 μm alumina, rinsed with distilled water, and wiped dry using a Kimwipe. Reported potentials are referenced against Ag/AgCl (3.0 M NaCl). Peak currents (i_p) were estimated with respect to the extrapolated baseline current as described elsewhere.[29] Under these conditions, the ferrocene/ferrocenium (FcH/FcH^+) couple occurs at 0.45 V.

Emission spectra were recorded using a SPEX Fluorolog-3 fluorimeter equipped with a double emission monochromator and a single-excitation monochromator. 77 K glassy solutions were prepared by inserting a quartz EPR tube containing either a 4:1 EtOH:MeOH or a 2:1 MeOH:2-MeTHF solution of the complex into a liquid nitrogen-filled quartz-tipped finger Dewar. Emission spectra were corrected for instrumental response. Emission samples for lifetime measurements at 77 K were excited using the third harmonic (355 nm) of a Continuum Surelite II Nd:YAG with 4−6

(19) Sakamoto, S.; Fujita, M.; Kim, K.; Yamaguchi, K. *Tetrahedron* **2000**, *56*, 955−964.
(20) Kuehl, C. J.; Songping, D. H.; Stang, P. J. *J. Am. Chem. Soc.* **2001**, *123*, 9634−9641.
(21) Stang, P. J.; Cao, D. H. *J. Am. Chem. Soc.* **1994**, *116*, 4981−4982.
(22) Stang, P. J.; Cao, D. H.; Saito, S.; Arif, A. M. *J. Am. Chem. Soc.* **1995**, *117*, 6273−6283.
(23) Pfennig, B. W.; Mordas, C. J.; McCloskey, A.; Lockard, J. V.; Salmon, P. M.; Cohen, J. L.; Watson, D. F.; Bocarsly, A. B. *Inorg. Chem.* **2002**, *41*, 4389−4395.
(24) Balashev, K. P.; Khanukaeva, O. R. *Russ. J. Gen. Chem.* **2001**, *71*, 1149−1150.
(25) Meijer, M. D.; de Wolf, E.; Lutz, M.; Spek, A. L.; van Klink, G. P. M.; van Koten, G. *Organometallics* **2001**, *20*, 4198−4206.
(26) Gallasch, D. P.; Tiekink, E. R. T.; Rendina, L. M. *Organometallics* **2001**, *20*, 3373−3382.
(27) Jude, H.; Krause Bauer, J. A.; Connick, W. B. *Inorg. Chem* **2002**, *41*, 2275−2281.
(28) Jude, H.; Krause Bauer, J. A.; Connick, W. B. *Inorg. Chem.* **2004**, *43*, 725−733.
(29) Kissinger, P. T.; Heineman, W. R. *J. Chem. Educ.* **1983**, *60*, 702−706.

ns pulse widths or 420 nm light from a Continuum Panther optical parametric oscillator pumped with the third harmonic of a Continuum Surelite II Nd:YAG laser. Emission transients were detected using a modified PMT connected to a Tektronix TDS580D oscilloscope and modeled using in-house software on a Microsoft Excel platform. Under these conditions, the emission decay of [Ru(2,2′-bipyridine)$_3$]Cl$_2$ in 4:1 EtOH:MeOH 77 K glassy solution was single exponential corresponding to a 5.1 μs lifetime, as expected.[30]

[(Pt(pip$_2$NCN))$_2$(μ-pyz)](CF$_3$SO$_3$)$_2$. A mixture of silver triflate (0.026 g, 0.1 mmol) and Pt(pip$_2$NCN)Cl (0.05 g, 0.1 mmol) in 15 mL of acetone was stirred for 30 min at room temperature. The resulting AgCl precipitate was removed by vacuum filtration through Celite. After addition of pyz (0.004 g, 0.05 mmol), the filtrate was stirred for 5 h, and the solvent was removed by rotary evaporation. The yellow solid was dissolved in CH_2Cl_2, and diethyl ether was added to induce precipitation. The product was washed with diethyl ether and dried. Yield: 0.037 g, 57%. Anal. Calcd for [$C_{40}H_{58}N_6Pt_2$](CF$_3$SO$_3$)$_2$: C, 38.47; H, 4.46; N, 6.41. Found: C, 38.24; H, 4.51; N, 6.28. ^{1}H NMR (CDCl$_3$, δ): 1.25−1.80 (24H, m, CH_2), 3.03 (8H, m, CH_2), 3.32 (8H, m, CH_2), 4.40 (8H, s with Pt satellites, $J_{H-Pt} = 52$ Hz, benzylic CH_2), 6.93 (4H, d, CH), 7.08 (2H, t, CH), 9.49 (4H, s, CH).

The BF_4^- salt ([(Pt(pip$_2$NCN))$_2$(μ-pyz)](BF$_4$)$_2$) was prepared by the same procedure as [(Pt(pip$_2$NCN))$_2$(μ-pyz)](CF$_3$SO$_3$)$_2$, substituting silver tetrafluoroborate for silver triflate. Yield: 0.034 g, 58%. Anal. Calcd for [$C_{40}H_{58}N_6Pt_2$](BF$_4$)$_2$: C, 40.49; H, 4.93; N, 7.08. Found: C, 40.05; H, 4.83; N, 6.97.

[(Pt(pip$_2$NCN))$_2$(μ-bpa)](CF$_3$SO$_3$)$_2$. This was prepared by the same procedure as for [(Pt(pip$_2$NCN))$_2$(μ-pyz)](CF$_3$SO$_3$)$_2$, substituting the appropriate starting materials: Pt(pip$_2$NCN)Cl (0.100 g, 0.2 mmol), silver triflate (0.051 g, 0.2 mmol), and bpa (0.018 g, 0.1 mmol). Yield: 0.107 g, 76%. Anal. Calcd for [$C_{48}H_{66}N_6Pt_2$](CF$_3$SO$_3$)$_2$·2H$_2$O: C, 41.38; H, 4.86; N, 5.79. Found: C, 41.26; H, 4.75; N, 5.82. ^{1}H NMR (CDCl$_3$, δ): 1.25−1.35 (16H, m, CH_2), 1.60−1.80 (8H, m, CH_2), 2.93 (8H, m, CH_2), 3.27 (12H, m, piperidyl and bridging CH_2), 4.38 (8H, s, benzylic CH_2), 6.91 (4H, d, CH), 7.06 (2H, t, CH), 8.01 (4H, d, CH), 8.77 (4H, d, CH).

[(Pt(pip$_2$NCN))$_2$(μ-bpe)](CF$_3$SO$_3$)$_2$. This was prepared by the same procedure as for [(Pt(pip$_2$NCN))$_2$(μ-pyz)](CF$_3$SO$_3$)$_2$, substituting the appropriate starting materials: Pt(pip$_2$NCN)Cl (0.110 g, 0.22 mmol), silver triflate (0.056 g, 0.22 mmol), and bpe (0.020 g, 0.11 mmol). Yield: 0.085 g, 55%. Anal. Calcd for [$C_{48}H_{64}N_6Pt_2$](CF$_3$SO$_3$)$_2$: C, 42.49; H, 4.57; N, 5.95. Found: C, 42.56; H, 4.59; N, 6.07. ^{1}H NMR (CDCl$_3$, δ): 1.25−1.35 (16H, m, CH_2), 1.60−1.80 (8H, m, CH_2), 2.94 (8H, m, CH_2), 3.28 (8H, m, CH_2), 4.39 (8H, s, benzylic CH_2), 6.92 (4H, d, CH), 7.07 (2H, m, CH), 7.97 (2H, s, bridging CH), 8.31 (4H, d, CH), and 8.82 (4H, d, CH).

X-ray Crystallography. Yellow plates of [(Pt(pip$_2$NCN))$_2$(μ-pyz)](CF$_3$SO$_3$)$_2$ were grown by slow evaporation of a CH_2Cl_2/$CHCl_3$ solution. Crystals of [(Pt(pip$_2$NCN))$_2$(μ-bpe)](CF$_3$SO$_3$)$_2$·2CH_2Cl_2 were obtained as colorless rods from CH_2Cl_2/hexanes/Et_2O. Diffraction data for [(Pt(pip$_2$NCN))$_2$(μ-pyz)](CF$_3$SO$_3$)$_2$ were collected at 150 K using a Bruker SMART6000 CCD diffractometer, and data for [(Pt(pip$_2$NCN))$_2$(μ-bpe)](CF$_3$SO$_3$)$_2$·2CH_2Cl_2 were collected at 150 K using a Bruker SMART 1K CCD diffractometer, both instruments utilizing graphite-monochromated Mo Kα radiation ($\lambda = 0.71073$ Å). For [(Pt(pip$_2$NCN))$_2$(μ-bpe)](CF$_3$SO$_3$)$_2$·2CH_2Cl_2, weakly diffracting data beyond 50° in 2θ were truncated. Data frames were processed using the SAINT program.[31] Intensities were corrected for Lorentz, polarization, and decay effects. Absorption and beam corrections based on the multiscan technique were applied using SADABS.[32] The structures were solved using SHELXTL[33] and refined by full-matrix least squares on F^2.

Table 1. Crystallographic Data and Structural Refinement Details for [(Pt(pip$_2$NCN))$_2$(μ-pyz)](CF$_3$SO$_3$)$_2$ and [(Pt(pip$_2$NCN))$_2$(μ-bpe)](CF$_3$SO$_3$)$_2$·2CH_2Cl_2

	[(Pt(pip$_2$NCN))$_2$(μ-pyz)](CF$_3$SO$_3$)$_2$	[(Pt(pip$_2$NCN))$_2$(μ-bpe)](CF$_3$SO$_3$)$_2$·2CH_2Cl_2
formula	[$C_{40}H_{58}N_6Pt_2$](CF$_3$SO$_3$)$_2$	[$C_{48}H_{64}N_6Pt_2$](CF$_3$SO$_3$)$_2$·2CH_2Cl_2
fw, g/mol	1311.24	1583.22
space group	$P\bar{1}$	$P2_1/c$
a, Å	12.5240(5)	10.1288(6)
b, Å	14.1570(6)	16.3346(9)
c, Å	14.2928(6)	17.4764(10)
α, deg	106.458(1)	90
β, deg	92.527(1)	90.882(2)
γ, deg	106.880(1)	90
V, Å^3	2303.46(17)	2891.1(3)
Z	2	2
ρ_{calc}, g cm^{-3}	1.891	1.819
T, K	150(2)	150(2)
radiation, Å	0.71073	0.71073
no. reflns collected	31588	14728
no. indpt reflns	11310	5083
GOF on F^2	1.059	1.028
R1/wR2 [$I > 2\sigma(I)$][a]	0.0341/0.0900	0.0697/0.1139
R1/wR2 (all data)[a]	0.0428/0.0959	0.1474/0.1369

[a] $R_1 = \sum||F_o| - |F_c||/\sum|F_o|$, wR2 = $[\sum w(F_o^2 - F_c^2)^2/\sum w(F_o^2)^2]^{1/2}$.

For all compounds, non-hydrogen atoms were located directly by successive Fourier calculations and refined anisotropically. Ligand H atoms were either located directly or calculated on the basis of geometric criteria and were treated with a riding model in subsequent refinements. The isotropic displacement parameters for the H atoms were defined as a times U_{eq} of the adjacent atom, where $a = 1.5$ for $-CH_3$ and 1.2 for all others.

For [(Pt(pip$_2$NCN))$_2$(μ-pyz)](CF$_3$SO$_3$)$_2$, one triflate anion is severely disordered, and the geometry of that anion was restrained to be similar to that of the well-behaved triflate. The highest residual electron density peaks are near the badly disordered triflate. Compound [(Pt(pip$_2$NCN))$_2$(μ-bpe)](CF$_3$SO$_3$)$_2$ crystallizes with two CH_2Cl_2 molecules in the lattice. Analysis of the intensity behavior for a number of reflections is consistent with monoclinic symmetry. Additionally, attempts at resolving potential twinning (β angle near 90°) by inclusion of a suitable twin law caused the refinement and metrical parameters to substantially worsen. One benzylic carbon (C13) is disordered, and the occupancies for C13A and C13B were set at 0.5. The anisotropic displacement parameters for piperidyl atoms, N2 and C13B, were set equivalent to the better behaved N1 and C13A, respectively. Crystallographic data are summarized in Table 1.

Results and Discussion

Synthesis. As illustrated in Scheme 1, three new dimers were prepared from Pt(pip$_2$NCN)Cl using the strategy previously employed in the synthesis of (Pt(pip$_2$NCN))$_2$(μ-bpy)$^{2+}$.[28] Metathesis was accomplished by allowing the monomer starting material to react with one equivalent of a silver salt (e.g., $AgCF_3SO_3$) at room temperature. After re-

(30) Juris, A.; Belser, P.; Barigelletti, F.; von Zelewsky, A.; Balzani, V. *Inorg. Chem.* **1986**, *25*, 256−259.

(31) SMART (v5.054, v5.628) and SAINT (v5.A06, v6.28A) programs were used for data collection and processing, respectively. Bruker Analytical X-ray Solutions, Inc., Madison, WI.

(32) SADABS was used for the application of semiempirical absorption and beam corrections. G. M. Sheldrick, University of Göttingen, Germany.

(33) SHELXTL (v5.1, v6.1, v6.12) programs were used for the structure solution and generation of figures and tables. Neutral-atom scattering factors were used as stored in this package. Bruker Analytical X-ray Solutions, Inc., Madison, WI.

Scheme 1. Synthesis of $(Pt(pip_2NCN))_2(\mu\text{-pyz})^{2+}$, $(Pt(pip_2NCN))_2(\mu\text{-bpe})^{2+}$, $(Pt(pip_2NCN))_2(\mu\text{-bpa})^{2+}$, and $(Pt(pip_2NCN))_2(\mu\text{-bpy})^{2+}$ [a]

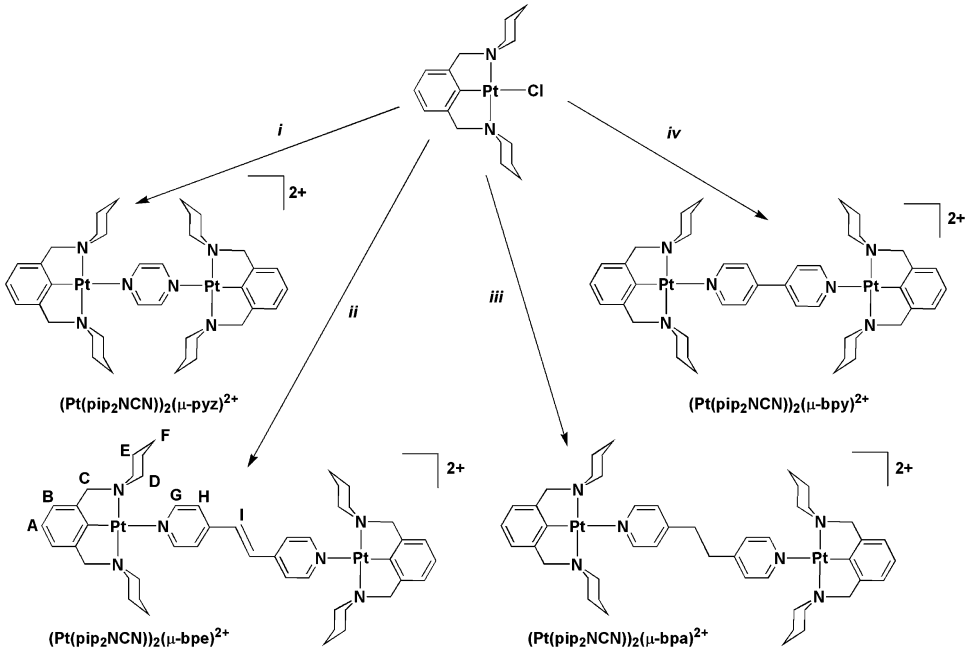

[a] (i) $AgCF_3SO_3$, pyrazine, acetone; (ii) $AgCF_3SO_3$, *trans*-1,2-bis(4-pyridyl)ethylene, acetone; (iii) $AgCF_3SO_3$, 1,2-bis(4-pyridyl)ethane, acetone; (iv) $AgCF_3SO_3$, 4,4′-bipyridine, acetone.

moval of silver chloride by filtration, 0.5 equiv of pyz, bpe, or bpa were added to give $(Pt(pip_2NCN))_2(\mu\text{-pyz})^{2+}$, $(Pt(pip_2NCN))_2(\mu\text{-bpe})^{2+}$, or $(Pt(pip_2NCN))_2(\mu\text{-bpa})^{2+}$, respectively. Each dimeric product was isolated in good yield (55−80%) as a triflate or tetrafluoroborate salt and fully characterized by ^{1}H NMR spectroscopy and elemental analysis.

The ^{1}H NMR spectra of the three new dimer products in $CDCl_3$ are qualitatively similar to those reported previously for platinum complexes with the pip_2NCN^- ligand.[27,28] A general labeling scheme for nonequivalent protons (A−I) is shown for the bpe-bridged dimer in Scheme 1. A doublet and triplet occur between 6.9 and 7.1 ppm, and these are assigned to the pip_2NCN^- phenyl protons (A, B). The resonance near 4.4 ppm is attributed to the benzylic protons (C). For the pyz- and bpy-bridged dimers, distinct ^{195}Pt satellites are resolved with J_{H-Pt} values of 52 and 47 Hz, respectively. The satellites appear as shoulders in the spectra of $(Pt(pip_2NCN))_2(\mu\text{-bpe})^{2+}$ and $(Pt(pip_2NCN))_2(\mu\text{-bpa})^{2+}$. Two characteristic multiplets between 2.9 and 4.1 ppm are assigned to the diastereotopic protons (D′ and D″) of the α-carbons of the piperidyl rings. Similarly, the aliphatic protons E and F are diastereotopic, accounting for the complexity of the splitting patterns further upfield. A pair of pyridyl doublet resonances with equal intensities occurs downfield of 8.0 ppm (G, H) for $(Pt(pip_2NCN))_2(\mu\text{-bpe})^{2+}$, $(Pt(pip_2NCN))_2(\mu\text{-bpa})^{2+}$, and $(Pt(pip_2NCN))_2(\mu\text{-bpy})^{2+}$, indicating that the two halves of the bridging ligand are equivalent. In the case of the pyz-bridged dimer, the pyz resonances appear as a singlet at 9.5 ppm. The bpe-bridged dimer also exhibits a singlet at 8.0 ppm (I) attributable to the protons of the olefin bridge, and the bpa-bridged dimer exhibits a singlet at 3.27 ppm (I) attributable to the protons of the aliphatic bridge. In $CDCl_3$, the latter resonance overlaps with a piperidyl CH_2 resonance (D).

In CD_3OD solution, the ^{1}H NMR spectra are qualitatively similar to those observed in deuterated chloroform. However, as previously noted for several related pyridyl monomers,[28] the spectra of all four compounds in alcohol solution are consistent with partial dissociation of the bridging ligands (<10%) at room temperature. In CD_3CN solution, dissociation is increased, and the spectra clearly exhibit resonances associated with the dimers, $Pt(pip_2NCN)(L)^+$ (L = pyz, bpa, bpy, or bpe) and a monomer complex, presumably having a water or acetonitrile ligand. In the case of unstable pyz-bridged Mn(I) dimers, poor Mn(I)/pyz π-back-bonding has been proposed to account for dissociation in solution.[34] However, this effect is likely less significant for these Pt(II) complexes, because the NCN^- ligand is not a strong competing π-acid and there are numerous examples of stable pyz-bridged Pt(II) assemblies.[2−5] A more significant factor is the strong trans-directing properties of the NCN^- ligand that tend to labilize the pyridyl ligand, as suggested for related systems.[28,35] This tendency has recently been exploited in the design of main-chain reversible polymers.[36]

Crystal Structures. The structures of the triflate salts of $(Pt(pip_2NCN))_2(\mu\text{-pyz})^{2+}$ and $(Pt(pip_2NCN))_2(\mu\text{-bpe})^{2+}$ were confirmed by X-ray crystallography. ORTEP diagrams of the cations are shown in Figures 1 and 2, and relevant data are summarized in Tables 1 and 2. No unusual intermolecular interactions are present in these crystals or crystals of $[(Pt(pip_2NCN))_2(\mu\text{-bpy})](CF_3SO_3)_2 \cdot {}^1/_2(CH_3)_2CO$,[28] and there is no evidence of the presence of water molecules.

For each complex, the pip_2NCN^- ligand is tridentate, and the conformation and metrical parameters for the

(34) Gross, R.; Kaim, W. *Inorg. Chem.* **1986**, *25*, 498−506.
(35) Schmulling, M.; Grove, D. M.; van Koten, G.; van Eldik, R.; Veldman, N.; Spek, A. L. *Organometallics* **1996**, *15*, 1384−1391.
(36) Yount, W. C.; Juwarker, H.; Craig, S. L. *J. Am. Chem. Soc.* **2003**, *125*, 15302−15303.

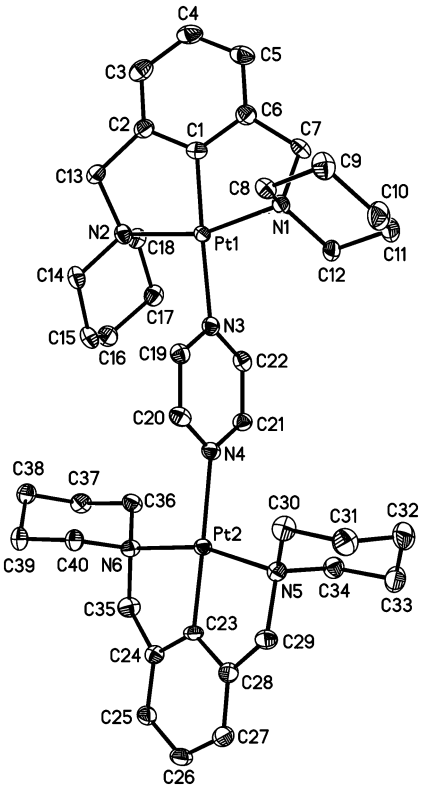

Figure 1. ORTEP diagram of the dication in crystals of $[(Pt(pip_2NCN))_2(\mu\text{-pyz})](CF_3SO_3)_2$. (Ellipsoids plotted at 50% probability, H atoms are omitted for clarity.)

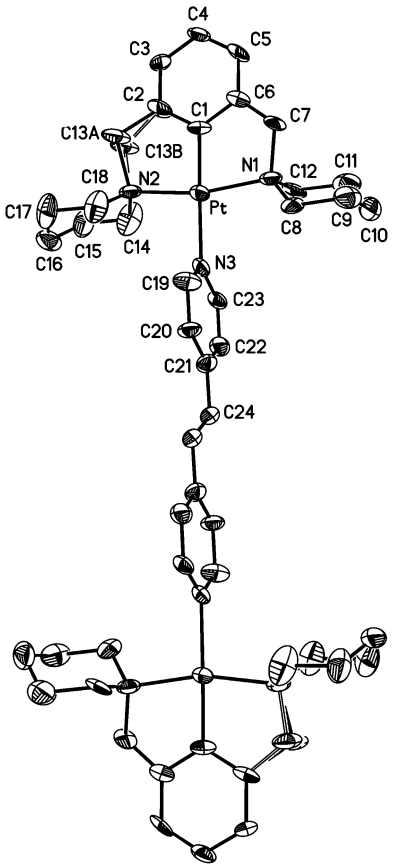

Figure 2. ORTEP diagram of the dication in crystals of $[(Pt(pip_2NCN))_2(\mu\text{-bpe})](CF_3SO_3)_2\cdot 2CH_2Cl_2$. (Ellipsoids plotted at 50% probability, H atoms are omitted for clarity.)

$Pt(pip_2NCN)$ units are in excellent agreement with those of related compounds.[27,28,37] Notably, the N(piperidyl)−Pt−N(piperidyl) angles ($(Pt(pip_2NCN))_2(\mu\text{-pyz})^{2+}$: 162.07(16), 164.47(16)°; $(Pt(pip_2NCN))_2(\mu\text{-bpe})^{2+}$: 164.8(4)°) are significantly less than the 180°, in keeping with the geometric preferences of the two five-membered chelate rings formed by the Pt atom and the pincer ligand.[27,28,35,38] These rings are slightly puckered, and the planar phenyl group is rotated slightly about the Pt−C bond, forming dihedral angles with the Pt coordination plane of 7.9/14.7° for $(Pt(pip_2NCN))_2(\mu\text{-pyz})^{2+}$ and 5.4° for $(Pt(pip_2NCN))_2(\mu\text{-bpe})^{2+}$.

When viewed end-on, the square planar subunits of the dimers are nearly eclipsed. The planar pyz and pyridyl (bpe) groups lie nearly perpendicular to each platinum coordination plane, forming dihedral angles of 83.3/89.8° and 85.2°, respectively. These angles are consistent with those observed for monomeric platinum pyridyl complexes with the pip_2NCN^- ligand (84.5−89.5°), as well as that observed for the bpy-bridged dimer (86.0°).[27,28] Similar angles also have been reported for pyz- and bpe-bridged molecular polyhedra (77.5−89.9°).[4,7] The nearly perpendicular orientation of the pyridyl and phenyl groups is consistent with steric considerations, as well as electronic effects, since the Pt−pyridine π-interactions do not directly compete with the Pt−phenyl π-interactions.[27,39,40]

Table 2. Selected Distances (Å) and Angles (deg) for $[(Pt(pip_2NCN))_2(\mu\text{-pyz})](CF_3SO_3)_2$ and $[(Pt(pip_2NCN))_2(\mu\text{-bpe})](CF_3SO_3)_2\cdot 2CH_2Cl_2$

	$[(Pt(pip_2NCN))_2(\mu\text{-pyz})](CF_3SO_3)_2$	$[(Pt(pip_2NCN))_2(\mu\text{-bpe})](CF_3SO_3)_2\cdot 2CH_2Cl_2$
Pt(1)−C(1)	1.936(5)	1.910(12)
Pt(1)−N(1)	2.094(4)	2.096(11)
Pt(1)−N(2)	2.126(4)	2.132(10)
Pt(1)−N(3)	2.132(4)	2.164(10)
Pt(2)−C(23)	1.922(5)	
Pt(2)−N(5)	2.099(4)	
Pt(2)−N(6)	2.098(4)	
Pt(2)−N(4)	2.144(4)	
C(1)−Pt(1)−N(1)	81.36(19)	81.7(5)
C(1)−Pt(1)−N(2)	80.77(19)	84.2(5)
N(1)−Pt(1)−N(3)	96.45(16)	97.1(4)
N(2)−Pt(1)−N(3)	101.41(16)	97.1(4)
C(1)−Pt(1)−N(3)	177.76(18)	178.3(5)
N(1)−Pt(1)−N(2)	162.07(16)	164.8(4)
C(23)−Pt(2)−N(5)	82.71(19)	
C(23)−Pt(2)−N(6)	81.76(19)	
N(5)−Pt(2)−N(4)	97.96(16)	
N(6)−Pt(2)−N(4)	97.55(16)	
C(23)−Pt(2)−N(4)	178.70(19)	
N(5)−Pt(2)−N(6)	164.47(16)	

The Pt−N(bpe) distance for the bpe-bridged dimer (2.164(10) Å) is somewhat longer than that observed for related molecular triangles and squares (2.09−2.14 Å).[7] However, the Pt−N(pyz) distances (2.132(4), 2.144(4) Å) are in good agreement with those observed for the molecular triangle $[(Pt(PMe_3)_2(\mu\text{-pyz}))_3](CF_3SO_3)_6\cdot 3CH_3NO_2$ (2.11−2.14 Å).[4]

(37) Jude, H.; Krause Bauer, J. A.; Connick, W. B. *J. Am. Chem. Soc.* **2003**, *125*, 3446−3447.
(38) Donkervoort, J. G.; Vicario, J. L.; Jastrzebski, J. T. B. H.; Smeets, W. J. J.; Spek, A. L.; van Koten, G. *J. Organomet. Chem.* **1998**, *551*, 1−7.
(39) Grove, D. M.; van Koten, G.; Ubbels, H. J. C.; Vrieze, K.; Niemann, L. C.; Stam, C. H. *J. Chem. Soc., Dalton Trans.* **1986**, *4*, 717−724.

Overall, these distances are consistent with the strong trans-directing properties of the pip_2NCN^- ligand.[28] For example, the Pt−N(pyz) distances are comparable to the Pt−N(py) distance observed for pyridine (py) situated trans to a phenyl group in *cis*-$Pt(Ph)_2(py)(CO)$ (2.140(4) Å)[41] but considerably longer than that found for complexes with weaker trans-directing groups, such as *cis*-$Pt(py)_2Cl_2$ (2.01(1) 2.04(1) Å).[42] Interestingly, the Pt−N(pyz) distances are just slightly shorter (∼0.02 Å) than the Pt−N(py) distance observed for $Pt(pip_2NCN)(py)^+$ (2.159(3) Å).[28] A comparable difference (0.045 Å) is observed for $((NH_3)_5Ru)_2(\mu\text{-pyz})^{4+}$ (2.013(3) Å)[43] and $(NH_3)_5Ru(py)^{2+}$ (2.058(8) Å).[44] Although the Pt−N distances are considerably longer than these Ru−N distances, in part because of trans influence, the trends in these distances are similar, reflecting the stronger π-back-bonding properties of the $(NH_3)_5M(pyz)^{2+}$ fragment (M = Pt or Ru) as compared to py. In the case of the bpe-bridged complex, π-back-bonding has no discernible impact on the remote bpe C24═C24′ distance (1.32(2) Å), which is comparable to those observed for the free ligand (bpe, 1.32 Å),[45] protonated bpe ($[bpeH_2](NO_3)_2$, 1.33/1.34 Å),[46] and *N*-methyl bpe^{2+} ($[N\text{-}Me_2\text{-}bpe]I_2$, 1.32 Å).[45]

Electrochemical Properties. Cyclic voltammograms were recorded for all four dimers in methylene chloride solution (0.1 M $TBAPF_6$). As noted for $Pt(pip_2NCN)(py)^+$,[28] the dimers do not oxidize at potentials less than 1.6 V. Similarly, as noted for $Pt(pip_2NCN)(L)^+$ monomers (L = py, Cl^-, Br^-, I^-),[28] the bpa-bridged dimer does not reduce at potentials >−1.8 V. In contrast, the other three dimers undergo a nitrogen heterocycle ligand-centered reduction at more positive potentials. For example, $(Pt(pip_2NCN))_2(\mu\text{-bpy})^{2+}$ undergoes a bipyridine-centered reduction at −1.22 V (ΔE_p = 61 mV, i_{pc}/i_{pa} = 1.4, 0.25 V/s).[28] In the case of $(Pt(pip_2NCN))_2(\mu\text{-pyz})^{2+}$, a nearly reversible one-electron reduction is observed at −0.88 V (ΔE_p = 66 mV, i_{pc}/i_{pa} = 1.4, 0.25 V/s), and a second irreversible reduction occurs at −1.5 V. For $(Pt(pip_2NCN))_2(\mu\text{-bpe})^{2+}$, a nearly reversible one-electron bpe-centered reduction is observed at −1.11 V (ΔE_p = 80 mV, i_{pc}/i_{pa} = 1.3, 0.25 V/s). In accord with this assignment, a bpe-centered reduction has previously been reported for $[(Pt(PEt_3)_2)_4(\mu\text{-bpe})_2(\mu\text{-anth})_2]^{4+}$ (anth = anthracene-1,8-diyl) near −1.36 V vs FcH/FcH^+ (ΔE_p = 67 mV, 0.2 V/s, 0.1 M $TBAPF_6$ in CH_3CN).[11] The ligand-centered reduction potentials of the dimers follow the order: μ-pyz (−0.88 V) > μ-bpe (−1.11 V) > μ-bpy (−1.22 V) > μ-bpa (<−1.8 V). The relative reduction potentials of the bpe, bpy, and bpa dimers are consistent with the free ligand reduction potentials of −1.80, −2.10, and <−2.3 V vs SCE (CH_2Cl_2, 0.1 M $TBAClO_4$), respectively.[47] In contrast, the pyz-bridged complex is significantly more easily reduced than expected from the free ligand reduction potential (<−2.3 V vs SCE), indicating that the unoccupied lowest π^* level is strongly stabilized by the electron-withdrawing $Pt(pip_2NCN)^+$ units. A similar observation has been reported for pyz-bridged Cr(0), Mo(0),[48] W(0),[47,49] Mn(I),[34] and Re(I) dimers,[49,50] as well as Re(I) squares.[51] For example, Zulu and Lees[47] observed a similar trend in reduction potentials for $(W(CO)_5)_2(\mu\text{-L})$ (0.1 M $TBAClO_4$ in CH_2Cl_2: μ-bpa (<−2.3 V) < μ-bpy (−1.30 V) < μ-bpe (−1.20 V) ≈ μ-pyz (−1.21 V vs SCE). The relative stabilization is likely greater for the platinum(II) dimers because of the increased acidity of the $Pt(pip_2NCN)^+$ fragment relative to $W(CO)_5$.

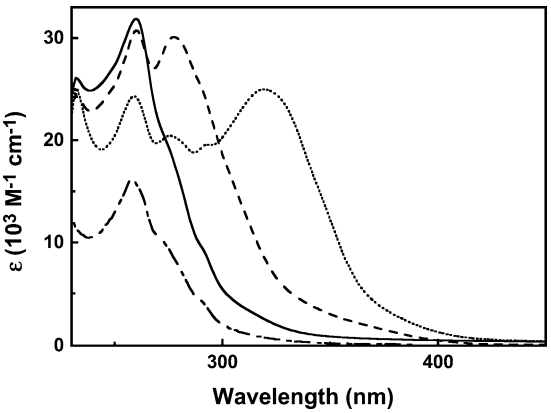

Figure 3. Room-temperature UV−visible absorption spectra in methylene chloride solution of $(Pt(pip_2NCN))_2(\mu\text{-bpe})^{2+}$ (···), $(Pt(pip_2NCN))_2(\mu\text{-bpa})^{2+}$ (—), $(Pt(pip_2NCN))_2(\mu\text{-bpy})^{2+}$ (− − −), and $Pt(pip_2NCN)(py)^+$ (- − - − -).

Absorption Spectroscopy. Salts of the bpa, bpy, and bpe dimers are colorless and dissolve in methylene chloride to give colorless solutions that absorb strongly in the UV region (Figure 3, Table 3). Salts of $(Pt(pip_2NCN))_2(\mu\text{-pyz})^{2+}$ are yellow and dissolve to give yellow solutions. The UV absorption spectra at wavelengths shorter than 300 nm exhibit charge-transfer bands similar to those of related complexes.[27,28] However, the absorption bands for the dimers exceed twice the intensity of the halide monomers ($Pt(pip_2NCN)X$ (X = Cl^-, Br^-, or I^-),[27] as expected for the occurrence of overlapping pyridyl ligand-centered transitions in this region. Similar absorption bands occur in the spectra of the free ligands (Table 3), as well as rhenium and ruthenium dimers.[52−54] Notably, $(Ru(NH_3)_5)_2(\mu\text{-bpe})^{6+}$ exhibits an intense ligand-centered absorption at 324 nm (27 500 M^{-1} cm^{-1}),[53] similar to that observed for $(Pt(pip_2NCN))_2(\mu\text{-bpe})^{2+}$ (320 nm, 25 000 M^{-1} cm^{-1}). Overall, the

(40) Albrecht, M.; Dani, P.; Lutz, M.; Spek, A. L.; van Koten, G. *J. Am. Chem. Soc.* **2000**, *122*, 11822−11833.
(41) Romeo, R.; Arena, G.; Scolaro, L. M.; Plutino, M. R.; Bruno, G.; Nicoló, F. *Inorg. Chem.* **1994**, *33*, 4029−4037.
(42) Colamarino, P.; Orioli, P. L. *J. Chem. Soc., Dalton Trans.* **1975**, 1656−1659.
(43) Fürholz, U.; Joss, S.; Bürgi, H. B.; Ludi, A. *Inorg. Chem.* **1985**, *24*, 943−948.
(44) Shin, Y.-G. K.; Szalda, D. J.; Brunschwig, B. S.; Creutz, C.; Sutin, N. *Inorg. Chem.* **1997**, *36*, 3190−3197.
(45) Vansant, J.; Smets, G.; Declercq, J. P.; Germain, G.; van Meerssche, M. *J. Org. Chem.* **1980**, *45*, 1557−1565.
(46) Felloni, M.; Blake, A. J.; Hubberstey, P.; Wilson, C.; Schröder, M. *CrystEngComm* **2002**, *4*, 483−495.
(47) Zulu, M. M.; Lees, A. J. *Inorg. Chem.* **1988**, *27*, 1139−1145.
(48) Pannell, K. H.; Iglesias, R. *Inorg. Chim. Acta* **1979**, *33*, L161−L162.
(49) Zulu, M. M.; Lees, A. J. *Organometallics* **1989**, *8*, 955−960.
(50) Lin, R.; Guarr, T. F. *Inorg. Chim. Acta* **1990**, *167*, 149−152.
(51) Slone, R. V.; Benkstein, K. D.; Belanger, S.; Hupp, J. T.; Guzei, I. A.; Rheingold, A. L. *Coord. Chem. Rev.* **1998**, *171*, 221−243.
(52) Rajendran, T.; Manimaran, B.; Lee, F.-Y.; Lee, G.-H.; Peng, S.-M.; Wang, C. M.; Lu, K.-L. *Inorg. Chem.* **2000**, *39*, 2016−2017.
(53) Sutton, J. E.; Taube, H. *Inorg. Chem.* **1981**, *20*, 3125−3134.
(54) Stanbury, D. M.; Gaswick, D.; Brown, G. M.; Taube, H. *Inorg. Chem.* **1983**, *22*, 1975−1982.

Table 3. Reduction Potentials,[a] Room-Temperature UV−Visible Absorption (CH_2Cl_2) Data and 77 K Emission Data

compound	absorption λ_{max}, nm (ϵ, M^{-1} cm^{-1})	emission (77 K) λ_{max}, nm (fwhm, cm^{-1}) glassy solution	emission (77 K) λ_{max}, nm (fwhm, cm^{-1}) solid state[d]	$E^{o\prime}$, V
$(Pt(pip_2NCN))_2(\mu\text{-pyz})^{2+}$	258, 270, 315, ∼368sh, ∼410sh[e]	∼510[b,f]	∼560[f]	−0.88
$(Pt(pip_2NCN))_2(\mu\text{-bpe})^{2+}$	259 (24300), 276 (20400), 292sh (19500), 320 (25000)	580, 638, 706, 780[b]	584, 642, 707, 780sh	−1.11
$(Pt(pip_2NCN))_2(\mu\text{-bpy})^{2+}$	260 (30750), 277 (30100), 291sh (24800), 305sh (15800)	433, 458, 485sh, 520sh[c]	449, 479, 507, 550sh	−1.22
$(Pt(pip_2NCN))_2(\mu\text{-bpa})^{2+}$	259 (31800), 276sh (18800), 292sh (8950)	638 (3600)[b]	650 (3800)	<−1.8

[a] Cyclic voltammograms were recorded in 0.1 M $TBAPF_6/CH_2Cl_2$ at 0.25 V/s and referenced vs Ag/AgCl. [b] 2:1 MeOH:2-MeTHF glassy solution. [c] 4:1 EtOH:MeOH glassy solution. [d] 77 K solid-state maxima for $CF_3SO_3^-$ salts. [e] Absorption maxima are reported for a 0.177 mM solution; maxima and intensities are concentration dependent. [f] λ_{ex} = 350 nm; the emission profiles are excitation-wavelength dependent (see text).

absorption profile of $(Pt(pip_2NCN))_2(\mu\text{-bpa})^{2+}$ is remarkably similar to that of $Pt(pip_2NCN)(py)^+$,[28] with twice the molar absorptivity, indicating that the electronic structures of the $Pt(pip_2NCN)(pyridyl)^+$ units are essentially unperturbed by dimer formation and that there is only weak communication between the metal centers. A similar observation has been made for $(W(CO)_5)_2(\mu\text{-bpa})$ and $W(CO)_5$(4-Mepy) (4-Mepy = 4-methylpyridine).[55,56]

At wavelengths to the red of the pyridyl-centered bands, the bpa, bpy, and bpe complexes exhibit tailing absorption profiles, attributable to ligand field and spin-forbidden charge-transfer transitions. It is also reasonable to anticipate relatively low-lying metal-to-ligand charge-transfer (MLCT) transitions in these spectra because of the low-lying pyridyl π^* levels. Electrochemical measurements suggest the MLCT energies should decrease along the ligand series: bpa > bpy > bpe. However, the ligand-centered $\pi-\pi^*$ charge-transfer energies also decrease along this series and may obscure the MLCT bands. In the case of the pyz-bridged dimer, the absorption spectrum of a 0.2 mM solution exhibits a band at 315 nm with apparent molar absorptivity of 9500 M^{-1} cm^{-1} and shoulders at 368 and 410 nm. These longer wavelength bands are absent from the spectra of monomeric pyridyl complexes[28] and cannot be reasonably attributed to ligand-centered transitions since the free and protonated bridging ligands (Table 3; $pyzH^+$(aq), pH < 0, λ > 300 nm, ϵ < 600 M^{-1} cm^{-1})[57] only absorb weakly in this region. Nor can these intense bands be reasonably assigned to ligand field transitions. A likely explanation is that these transitions have significant metal-to-ligand (pyz) charge-transfer character, in keeping with the notion of a low-lying pyz π^* level. The blue shift of these bands with respect to that observed for $(Ru(NH_3)_5)_2(\mu\text{-pyz})^{4+}$ (547 nm, 30 000 M^{-1} cm^{-1})[58] is consistent with the relative energies of MLCT states of Pt(II) and Ru(II) complexes.[59,60]

In contrast to the other three dimers, the absorption profile of $(Pt(pip_2NCN))_2(\mu\text{-pyz})^{2+}$ in CH_2Cl_2 is concentration dependent (Figure 4), and solutions of this compound do not obey Beer's law. As the dimer concentration is lowered from 0.2 to 0.01 mM, the apparent molar absorptivity of the 315 nm band (and longer wavelength shoulders) decreases, and that of the 258 nm band increases. The data are consistent with partial dissociation of $(Pt(pip_2NCN))_2(\mu\text{-pyz})^{2+}$ to form $Pt(pip_2NCN)(pyz)^+$ and a solvated adduct and/or aquo complex resulting from reaction with adventitious water. In support of this interpretation, titration of a 0.09 M solution of $(Pt(pip_2NCN))_2(\mu\text{-pyz})^{2+}$ with pyz increased dissociation, as indicated by a gradual decrease in intensity of the 315 nm band and an increase in the intensity of the 258 nm band (Figure 4 inset). The loss of intensity of the 315 nm and longer wavelength absorption bands indicates that the MLCT transitions of $Pt(pip_2NCN)(pyz)^+$ are shifted to shorter

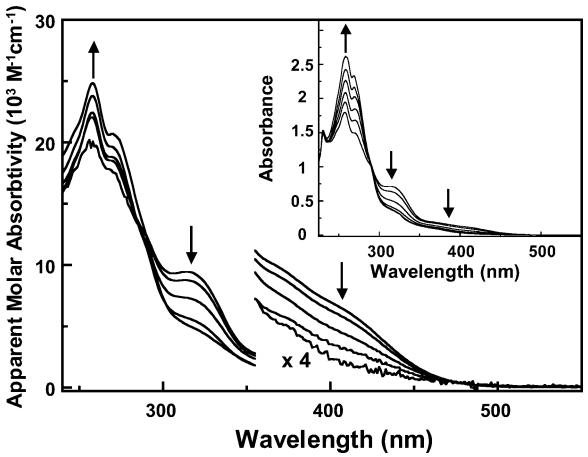

Figure 4. Apparent molar absorptivity of $[(Pt(pip_2NCN))_2(\mu\text{-pyz})](BF_4)_2$ in CH_2Cl_2 recorded with decreasing concentration: 1.77×10^{-4}, 8.85×10^{-5}, 3.54×10^{-5}, 1.77×10^{-5}, and 7.08×10^{-6} M. Inset: UV−visible absorption spectra recorded during titration of $[(Pt(pip_2NCN))_2(\mu\text{-pyz})](BF_4)_2$ (100 mL of 8.85×10^{-5} M) with 4×45 μL aliquots (0.5 equiv) of 0.1 M pyrazine. Free pyrazine only absorbs weakly at λ > 275 nm ($\epsilon \leq 600$ M^{-1} cm^{-1}).

(55) Gaus, P. L.; Boncella, J. M.; Rosengren, K. S.; Funk, M. O. *Inorg. Chem.* **1982**, *21*, 2174−2178.
(56) Wrighton, M. S.; Abrahamson, H. B.; Morse, D. L. *J. Am. Chem. Soc.* **1976**, *98*, 4105−4109.
(57) Peral, F.; Gallego, E. *Spectrochim. Acta, Part A* **2003**, *59*, 1223−1237.
(58) Creutz, C.; Taube, H. *J. Am. Chem. Soc.* **1969**, *91*, 3988−3989.
(59) For example, the lowest spin-allowed MLCT band for Pt(2,2′-bipyridine)Cl_2 (390 nm, DMF; Connick, W. B., Ph.D. Dissertation, California Institute of Technology, 1997) is shifted by 7600 cm^{-1} to the blue of that observed for Ru(2,2′-bipyridine)$_2Cl_2$ (553 nm, DMF; Vos, J. G.; Haasnoot, J. G.; Vos, G. *Inorg. Chim. Acta* **1983**, *71*, 155−162.).
(60) For D_{2h} symmetric $(Pt(pip_2NCN))_2(\mu\text{-pyz})^{2+}$, there are four spin-allowed and Laporte-allowed MLCT transitions involving the 5d(Pt) and lowest π^*(pyz) levels, although only three of these are fully allowed by symmetry.

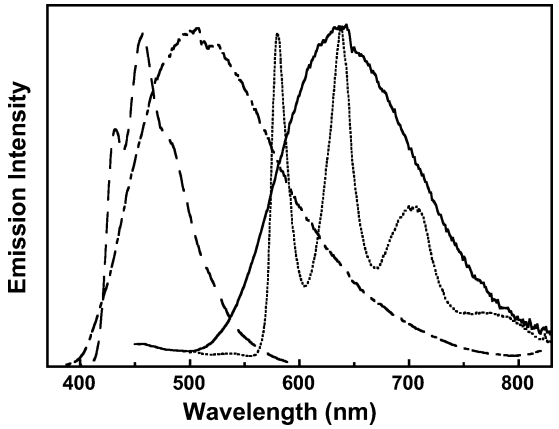

Figure 5. 77 K emission spectra in 2:1 MeOH:2-MeTHF ($(Pt(pip_2NCN))_2(\mu\text{-pyz})^{2+}$ (- − - − -, $\lambda_{ex} = 350$ nm)), $(Pt(pip_2NCN))_2(\mu\text{-bpe})^{2+}$ (•••, $\lambda_{ex} = 375$ nm)), $(Pt(pip_2NCN))_2(\mu\text{-bpa})^{2+}$ (—, $\lambda_{ex} = 300$ nm)) or 4:1 ethanol:methanol ($(Pt(pip_2NCN))_2(\mu\text{-bpy})^{2+}$ (− − −, $\lambda_{ex} = 300$ nm)) glassy solution. Intensities have been arbitrarily scaled.

wavelengths than those of the dimer, in keeping with the view that, when coordinated to $Pt(pip_2NCN)(pyz)^+$, the $Pt(pip_2NCN)^+$ fragment effectively acts as an electron-withdrawing subsitutent that stabilizes the π^* levels of the pyz ligand.

Emission Spectroscopy. Although none of these dimers is luminescent in fluid solution, each is emissive in rigid media. For example, salts of $(Pt(pip_2NCN))_2(\mu\text{-bpy})^{2+}$ exhibit yellow-green emission when irradiated with UV light at room temperature,[28] whereas salts of $(Pt(pip_2NCN))_2(\mu\text{-bpa})^{2+}$ and $(Pt(pip_2NCN))_2(\mu\text{-bpe})^{2+}$ exhibit weak red emissions. In contrast, salts of $(Pt(pip_2NCN))_2(\mu\text{-pyz})^{2+}$ exhibit remarkably intense yellow emission at room temperature. To investigate the origin of these properties, spectra of solid and dilute glassy solution samples (4:1 EtOH:MeOH and/or 2:1 MeOH:2-MeTHF) were recorded at 77 K (Figure 5, Table 3). The emission profiles of the bpe-, bpa-, and bpy-bridged dimers are concentration and excitation-wavelength independent, indicating that monomeric complexes or aggregates are not responsible for the observed spectra. However, frozen solution and solid-state emission profiles of $(Pt(pip_2NCN))_2(\mu\text{-pyz})^{2+}$ are excitation-wavelength dependent.

As previously reported,[28] the bpy-bridged dimer in 77 K 4:1 EtOH:MeOH glassy solution exhibits a structured, long-lived emission maximizing at 458 nm (21830 cm^{-1}, τ, 0.16 ms). The vibronic spacings of ~1000 and ~1400 cm^{-1} are consistent with a lowest bpy-centered, predominantly spin-forbidden $\pi-\pi^*$ excited state. The influence of the platinum centers is suggested by deviations in the emission spectrum from that of the free ligand, including a ~1000 cm^{-1} shift to lower energy, a slight broadening of the vibronic features, and differences in the Franck−Condon factors.[28]

The bpe-bridged dimer in 77 K 2:1 MeOH:2-MeTHF glassy solution also exhibits a highly structured emission profile, though shifted to considerably longer wavelengths with maxima at 580, 638, 706, and 780 nm. Although too weak for lifetime measurements, the emissions from solid-state and 77 K glassy solution samples clearly originate from a bpe-centered, predominantly spin-forbidden $\pi-\pi^*$ excited state. Under similar conditions, the emission spectrum of free bpe is dominated by a short-wavelength fluorescence centered at 405 nm, suggesting that platinum-induced spin−orbit coupling influences the photophysics of the bpe ligand. The vibronic progression (1300−1600 cm^{-1} spacings) and Franck−Condon factors of the dimer emission, as indicated by the Huang−Rhys ratio[61] ($I_{1,0}/I_{0,0} \approx 1$), are in excellent agreement with those of the free-ligand phosphorescence spectrum (77 K butyronitrile; 558, 608, 666 nm).[62] The first vibronic feature (~17 250 cm^{-1}) provides an estimate of the $^3(\pi-\pi^*)$ energy and is shifted by only ~650 cm^{-1} from that observed for the free ligand (~17 900 cm^{-1}). Thus, the accumulated data are consistent with slightly less perturbation of the emissive $\pi-\pi^*$ state than found for the bpy-bridged complex, in keeping with our earlier conclusion that the lowest states involving orbitals of the $Pt(pip_2NCN)$ fragment lie at significantly higher energies (> 23 500 cm^{-1}).[28]

To our knowledge, this is the first report of bpe-centered $^3(\pi-\pi^*)$ emission from a metal complex, though our results are in qualitative agreement with observations for several other complexes. As noted for the bpe-bridged dimer, several Re(I) monomers and squares with bpe ligands have been reported to be nonemissive in fluid solution[51,63−66] or exhibit short-lived, high-energy fluorescence.[52,67] Excited *trans*-stilbene and stilbene-like derivatives, such as bpe, are susceptible to nonradiative relaxation by forming a twisted triplet state (^{3}p).[64,68−70] In rigid media, the barrier to forming the ^{3}p state is expected to be significantly increased, accounting for our ability to detect emission from the bpe $^3(\pi-\pi^*)$ state. In contrast, several ruthenium and tungsten complexes with bpe ligands exhibit short-lived ^{3}MLCT emission in fluid solution.[47,49,71] In the case of the ruthenium systems, the emissions maximize near 700 nm,[71] suggesting that the ^{3}MLCT state lies well below the bpe-centered $^3(\pi-\pi^*)$ state. In contrast, Zulu and Lees[47,49,71] found that emissions from $W(CO)_5$(bpe) and $(W(CO)_5)_2(\mu\text{-bpe})$ maximize at 549 and 560 nm, respectively, and these authors noted that these complexes have lower quantum yields and shorter lifetimes than related compounds.[47,49] In conjunction with our results, these observations suggest that the lowest ^{3}MLCT and bpe $^3(\pi-\pi^*)$ states of the W(0) complexes lie in close proximity, and it is conceivable that the emissive

(61) Huang, K.; Rhys, A. *Proc. R. Soc. London* **1950**, *204A*, 406.
(62) Görner, H. *J. Phys. Chem.* **1989**, *93*, 1826−1832.
(63) Itokazu, M. K.; Polo, A. S.; de Faria, D. L. A.; Bignozzi, C. A.; Iha, N. Y. M. *Inorg. Chim. Acta* **2001**, *313*, 149−155.
(64) Dattelbaum, D. M.; Itokazu, M. K.; Iha, N. Y. M.; Meyer, T. J. *J. Phys. Chem. A* **2003**, *107*, 4092−4095.
(65) Wenger, O. S.; Henling, L. M.; Day, M. W.; Winkler, J. R.; Gray, H. B. *Inorg. Chem.* **2004**, *43*, 2043−2048.
(66) Slone, R. V.; Hupp, J. T.; Stern, C. L.; Albrecht-Schmitt, T. E. *Inorg. Chem.* **1996**, *35*, 4096−4097.
(67) Manimaran, B.; Rajendran, T.; Lu, Y.-L.; Lee, G.-H.; Peng, S.-M.; Lu, K.-L. *J. Chem. Soc., Dalton Trans.* **2001**, 515−517.
(68) Saltiel, J.; Charlton, J. L.; Mueller, W. B. *J. Am. Chem. Soc.* **1979**, *101*, 1347−1348.
(69) Saltiel, J.; Marchand, G. R.; Kirkor-Kaminska, E.; Smothers, W. K.; Mueller, W. B.; Charlton, J. L. *J. Am. Chem. Soc.* **1984**, *106*, 3144−3151.
(70) Schanze, K. S.; Lucia, L. A.; Cooper, M.; Walters, K. A.; Ji, H.-F.; Sabina, O. *J. Phys. Chem. A* **1998**, *102*, 5577−5584.
(71) Curtis, J. C.; Bernstein, J. S.; Meyer, T. J. *Inorg. Chem.* **1985**, *24*, 385−397.

^{3}MLCT state is thermally populated from a lowest bpe-centered state.

The emission spectra of 77 K solid-state and glassy solution samples of $(Pt(pip_2NCN))_2(\mu\text{-bpa})^{2+}$ are distinctly different from those of the bpe-bridged dimer. Excitation of glassy solutions at 300 nm results in a weak, broad, low-energy, and Gaussian-shaped emission centered near 640 nm (15 630 cm^{-1}) with a full-width at half-maximum (fwhm) of 3600 cm^{-1} (Figure 5.) In the solid state, the emission maximum (650 nm) is shifted to a slightly longer wavelength. The excitation spectra are in good agreement with the solution absorption data, and at longer wavelengths, a weak band is resolved at 367 nm, similar to that observed for $Pt(pip_2NCN)(py)^+$ (365 nm). Overall, the emission spectrum is strikingly similar to ^{3}LF emission observed for the pyridine analogue (650 nm, fwhm = 3700 cm^{-1}, 77 K 4:1 EtOH:MeOH),[28] and a similar assignment is made here. The large Stokes shift (11 600 cm^{-1}) of the emission maximum from the lowest-energy excitation feature and the broad emission bandshape are consistent with an excited state, having an optimum geometry very different from the ground state, as expected for population of the $Pt(d_{x^2-y^2})$ antibonding level. These conclusions are in accord with our earlier suggestion that bonding of pip_2NCN^- and a pyridyl ligand to a Pt(II) center will result in a lowest ^{3}LF state $\geq$ 23 500 cm^{-1},[28] but still below the energy of the lowest pyridine-centered $\pi-\pi^*$ state ($\sim$29 650 cm^{-1}).

By comparison to the other dimers and previously investigated monomers, emissions from samples of the pyz-bridged dimer are remarkably intense. Excitation of 77 K glassy solution samples at 350 nm results in a broad and very intense emission centered near 510 nm (Figure 5). The solid-state emission maximum of the BF_4^- salt is shifted to longer wavelengths ($\sim$560 nm). In both cases, the emission maximum is excitation-wavelength dependent. For example, the 77 K solid-state emission maximum occurs at 550 and 568 nm for excitation wavelengths of 300 and 430 nm, respectively. When 77 K glassy solutions (2:1 MeOH:2-MeTHF) are excited at 375 nm, the emission can be reasonably modeled with one Gaussian function (λ_{max} = 505 nm, fwhm = 5200 cm^{-1}). However, as the excitation wavelength is tuned from 375 to 300 nm, a low-energy shoulder emerges (Figure 6), and two Gaussian functions are required to fit the resulting spectrum (λ_{max} = 502 nm, fwhm = 5200 cm^{-1}; λ_{max} = 640 nm, fwhm = 3800 cm^{-1}). In addition, excitation between 300 and 325 nm results in a weak, highly structured emission near 400 nm (Figure 6). The accumulated data are suggestive of three different emitting species. One absorbs at wavelengths as long as 430 nm, whereas the remaining two species absorb comparatively weakly at wavelengths $\geq$375 and $\geq$325 nm, respectively. The dependence of the emission maximum on excitation wavelength is consistent with variations in the contributions of the three emitting species to the overall spectrum.

The excitation dependence of the dilute glassy solution emission further corroborates the tendency of the pyrazine dimer to dissociate in solution, most likely forming $Pt(pip_2NCN)(pyz)^+$ and a solvated adduct. The long wavelength component of the emission from glassy solution samples is almost coincident with the ^{3}LF emissions of $Pt(pip_2NCN)(py)^+$ (650 nm, fwhm = 3700 cm^{-1}) and $Pt(pip_2NCN)(H_2O)^+$ (λ_{max} = 634 nm, fwhm = 3700 cm^{-1}). Although we have not been able to prepare pure samples of $Pt(pip_2NCN)(pyz)^+$, we anticipate that the crystal field splitting for this complex will be similar to that of $Pt(pip_2NCN)(py)^+$. On the other hand, the weak, structured emission at 400 nm resulting from 300 to 325 nm excitation is characteristic of free pyrazine (λ_{max} = 390, 400, 410, 420 nm), indicating that $Pt(pip_2NCN)(pyz)^+$ further dissociates, in analogy to observations for $Pt(pip_2NCN)(py)^+$.[28] Upon excitation at longer wavelengths where pyrazine does not strongly absorb (e.g., 350 nm), the structured pyrazine emission is absent.

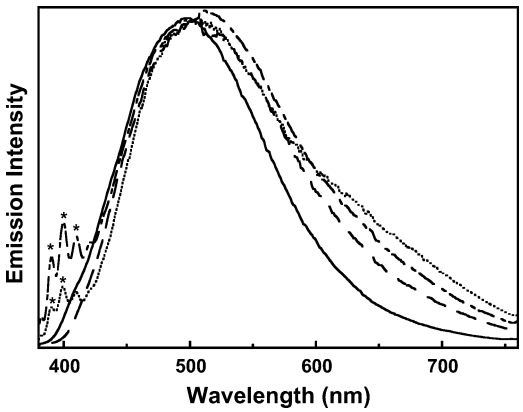

Figure 6. 77 K glassy solution emission (2:1 MeOH:2-MeTHF) spectra of $(Pt(pip_2NCN))_2(\mu\text{-pyz})^{2+}$ showing the dependence of the emission on excitation wavelength: λ_{ex} = 300 (···), 325 (- − - − -), 350 (− − −), and 375 nm (———). Intensities have been arbitrarily scaled. Emission maxima for free pyrazine is denoted by *.

The preceding leads to the conclusion that the broad, intense emission centered near 510 nm arises from the $(Pt(pip_2NCN))_2(\mu\text{-pyz})^{2+}$ dimer, which absorbs at wavelengths as long as 430 nm. The predominantly spin-forbidden character of the emission was verified by luminescence decay measurements. Emission decay traces from 77 K solid-state samples of the BF_4^- and $CF_3SO_3^-$ salts excited at 355 nm could not be adequately modeled with a single exponential function but required a biexponential function to obtain a reasonable fit (2, 4 μs components in $\sim$10:1 intensity ratio) as expected for partial ligand substitution. Therefore, in addition to the dimer, $Pt(pip_2NCN)(pyz)^+$ and $Pt(pip_2NCN)(H_2O)^+$ likely contribute to the emission decay. Interestingly, decay traces for solid $[(Pt(pip_2NCN))_2(\mu\text{-pyz})](CF_3SO_3)_2$ excited at 420 nm were adequately modeled by a single exponential function (3 μs), as would be expected for selective excitation of the dimer. Qualitatively, the emission is much more intense than the ^{3}LF and $^3(\pi-\pi^*)$ emissions previously observed for this class of complexes, and neither of these assignments is appealing. The emission maximum ($\sim$20 000 cm^{-1}, 500 nm) occurs at significantly higher energies than those observed for complexes with lowest ^{3}LF excited states (e.g., $Pt(pip_2NCN)Cl$, 14 200 cm^{-1}; $Pt(pip_2NCN)(py)^+$, 15 400 cm^{-1}).[27,28] In addition, the emission onset is shifted by $\sim$2000 cm^{-1} to lower energy of the free ligand $n-\pi^*$ emission, and the band lacks the structure expected

for a $^3(\pi-\pi^*)$ pyrazine-centered emission.[72,73] The lifetime also is significantly shorter than observed for related complexes with lowest pyridyl-centered $^3(\pi-\pi^*)$ excited states (e.g., $(Pt(pip_2NCN))_2(\mu\text{-bpy})^{2+}$, 0.16 ms).[28] These data are consistent with a significantly faster rate of radiative decay for the pyz dimer, as expected for increased involvement of the heavy metal center in the transition. For these reasons, and bearing in mind that both electrochemical and UV−visible absorption measurements point to stabilization of the pyrazine π^* level as compared to the pyridyl complexes, we tentatively assign the 510 nm emission of the dimer as having significant MLCT character.

Conclusions

This study, in conjunction with our earlier work,[27,28] illustrates how ligand modifications can provide remarkable control over the electronic structures and photophysics of metal complexes. Generally speaking, the strategy developed here for tuning electronic properties is complementary to an approach that uses variations in para substituents of the NCN^- ligand to influence electron density at the platinum center, as recently demonstrated by van Koten, Konigsberger, and co-workers.[74] In the present case, the emission properties of a series of dimers suggest the intriguing notion that it is possible to tune between the lowest ^{3}LF, $^3(\pi-\pi^*)$, and ^{3}MLCT states of $(Pt(pip_2NCN))_n(L)^{n+}$ complexes ($n = 1, 2$) by careful selection of L. The notion of ^{3}MLCT emission from the pyz dimer suggests the lowest ^{3}LF and $^3(\pi-\pi^*)$ states for this complex lie at higher energies than the emission onset ($\sim$25 000 cm^{-1}). At present, the orbital character of the MLCT state is uncertain; however, it is noteworthy that the emission is remarkably more intense than the pyridyl-centered $^3(\pi-\pi^*)$ emissions observed for $(Pt(pip_2NCN))_2(\mu\text{-bpy})^{2+}$, $(Pt(pip_2NCN))_2(\mu\text{-bpe})^{2+}$, and $Pt(pip_2NCN)(phpy)^+$. This situation contrasts with observations for platinum(II) diimine complexes, which tend to exhibit $^3(\pi-\pi^*)$ and ^{3}MLCT emissions with more comparable intensities and lifetimes within roughly an order of magnitude of one another.[75−77] In the case of the platinum(II) pip_2NCN^- complexes with lowest pyridyl $^3(\pi-\pi^*)$ excited states, the emissions are only weakly perturbed from those of the free ligand, and the lifetimes tend to be longer than those of their platinum(II) diimine and terpyridyl counterparts. These results are consistent with complexes such as $(Pt(pip_2NCN))_2(\mu\text{-bpy})^{2+}$, $(Pt(pip_2NCN))_2(\mu\text{-bpe})^{2+}$, and $Pt(pip_2NCN)(phpy)^+$ having relatively pure lowest intraligand excited states. The intensity of the emission from the pyz dimer is suggestive of an orbitally allowed excited state possibly having $d_{xy}\rightarrow p^*(pyz)$ character, which is expected to have a large transition dipole from overlap considerations.

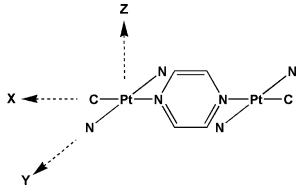

Acknowledgment. Funding for the SMART6000 CCD diffractometer was through NSF-MRI Grant CHE-0215950. Diffraction data on the SMART 1K CCD were collected through the Ohio Crystallographic Consortium, funded by the Ohio Board of Regents 1995 Investment Fund (CAP-075) and located at the University of Toledo, Instrumentation Center in A&S, Toledo, OH 43606. W.B.C. thanks the National Science Foundation (CHE-0134975) for their generous support and the Arnold and Mabel Beckman Foundation for a Young Investigator Award. H.J. and W.B.C. are grateful to the University of Cincinnati University Research Council for summer research fellowships. H.J. thanks the University of Cincinnati Department of Chemistry for the Stecker Fellowship, the Link Foundation for an Energy Fellowship, and the University of Cincinnati for a Distinguished Dissertation Fellowship. We thank Drs. M. J. Baldwin and M. J. Goldcamp for helpful discussions and expert technical assistance.

Supporting Information Available: Tables of crystallographic data, structure refinement details, atomic coordinates, interatomic distances and angles, anisotropic displacement parameters, and calculated hydrogen parameters (CIF). This material is available free of charge via the Internet at http://pubs.acs.org.

IC049166H

(72) Shimada, R. *Spectrochim. Acta* **1961**, *17*, 14−29.
(73) Grabowska, A.; Pakula, B. *Chem. Phys. Lett.* **1967**, *1*, 369−372.
(74) Tromp, M.; van Bokhoven, J. A.; Slagt, M. Q.; Gebbink, R. J. M. K.; van Koten, G.; Ramaker, D. E.; Koningsberger, D. C. *J. Am. Chem. Soc.* **2004**, *126*, 4090−4091.
(75) Miskowski, V. M.; Houlding, V. H. *Inorg. Chem.* **1989**, *28*, 1529−1533.
(76) Miskowski, V. M.; Houlding, V. H.; Che, C.-M.; Wang, Y. *Inorg. Chem.* **1993**, *32*, 2518−2524.
(77) Connick, W. B.; Miskowski, V. M.; Houlding, V. H.; Gray, H. B. *Inorg. Chem.* **2000**, *39*, 2585−2592.